Geomorphology 195 (2013) 27–44

Contents lists available at SciVerse ScienceDirect

Geomorphology

journal homepage: www.elsevier.com/locate/geomorph

Development and growth of recently-exposed fumarole fields near Mullet Island, Imperial County, California

David K. Lynch [a,b,*], Kenneth W. Hudnut [a], Paul M. Adams [b,1]

[a] United States Geological Survey, 525 South Wilson Ave., Pasadena, CA 91106-3212, United States
[b] Thule Scientific, 22914 Portage Circle Drive, Topanga, CA 90290, United States

ARTICLE INFO

Article history:
Received 12 April 2011
Received in revised form 1 April 2013
Accepted 9 April 2013
Available online 24 April 2013

Keywords:
Gryphon
Mud volcano
Mud pot
Salton Sea
Salton Trough
Fumarole

ABSTRACT

New field observations, aerial surveys, LiDAR measurements and laboratory studies of mud samples (2006 to 2012) are reported of several formerly submerged fumarole complexes that are presently undergoing surface exposure as the Salton Sea level drops. Some remain submerged as of this writing (2012). The fumarole fields range in area from 1000 to ~50,000 m^2. They consist of hundreds of warm to boiling hot gryphons (mud volcanoes), salses (mud pots), and countless active gas vents. Unusually-shaped mud volcanoes in the form of vertical tubes with central vents were observed in many places. Since exposure began in ~2007, the surface morphology has changed dramatically, with a trend toward more and growing gryphons, larger mud pots and the development of sulfur vents. Chemical analysis of mud from several gryphons revealed the presence of the ammoniated sulfate minerals boussingaultite and lecontite among other more common sulfates. With other geothermal features, the fumaroles define a well-defined lineament marking the trace of a probable fault. A model for the development of gryphon morphology is presented.

1. Introduction

Mud volcanoes are formed by the upward migration of fluidized sediment driven by subsurface over-pressured gas. Rising viscous mud is forced upward though a narrow vent where it accumulates, creating a conical mound around the central conduit (Ives, 1951; Jakubov et al., 1971; Macdonald, 1982; Hovland et al., 1997; Delisle et al., 2002; Kopf, 2002; Martinelli and Behrouz, 2003; Planke et al., 2003; Etiope et al., 2004; Bonini, 2008, 2009; Mazzini et al., 2009a, b; Svensen et al., 2009; Onderdonk et al., 2011). The process is mechanically analogous to igneous volcanoes. Though some mud volcanoes can be hundreds of meters high, those smaller than about 2 m in height are called "gryphons". On the earth's surface where water is abundant, bubbling water sometimes stands in the calderas of gryphons, where they are termed "salses". Salses are often called "mud pots", and may vary in fluid content between water with small amounts of sediment to thick, viscous mud. Gryphons and salses associated with fumaroles and high geothermal gradients are "hot" (boiling and steaming) and emit gasses such as CO_2, H_2O, SO_2, H_2S, NH_3, and CH_4 (Dimitrov, 2002). Others are "cold" and emit primarily CO_2. Cold gryphons with central salses are sometimes termed "mound springs". Mud volcanoes are relatively rare geological structures and tend to occur at active plate margins like the Salton Trough (Dimitrov, 2002; Martinelli and Behrouz, 2003).

The Salton Trough is a topographic low in southern California and northern Baja & Sonora Mexico (Fuis and Mooney, 1990; Dangermond, 2003) representing a tectonically active, sedimentary pull apart basin (Elders et al., 1972; Mann et al., 1983; Lonsdale, 1989; Brothers et al., 2009; Gurbuz, 2010). Except for minor contributions from the surrounding mountains and aeolian sources, most of the sediments in the Salton Trough represent Colorado River sediments and are as thick as 6 km (Muffler and White, 1969). The structurally controlled depression lies in the transition between the right lateral San Andreas Fault system and a series of oblique spreading centers of the northern extension of the Gulf of California (Macdonald, 1982). It is dominated by a number of contiguous right lateral, right stepping (releasing) transform faults including the Imperial and Cerro Prieto faults (Magistrale, 2002; Meltzner et al., 2006) and those of the Sierra Cucapah in Mexico where the Mw 7.2 April 4th, 2010 El Mayor–Cucapah earthquake recently occurred (Hauksson et al., 2010).

Within the Salton Trough lies the Salton Sea Geothermal Field. Here the geothermal gradient averages ~0.3 °C/m (Younker et al., 1982; Elders and Cohen, 1983), reaching a maximum of 4.3 °C/m (Lee and Cohen, 1979), enough to support a number of commercial geothermal electricity generating plants. The high geothermal gradient is the result of a shallow magma body from one or more spreading centers (Lachenbruch et al., 1985; Schmitt and Vazquez, 2006). Extruded

* Corresponding author at: Thule Scientific, 22914 Portage Circle Drive, Topanga, CA 90290, United States. Tel./fax: +1 310 455 3335.
E-mail address: dave@caltech.edu (D.K. Lynch).
[1] Tel./fax: +1 310 455 3335.

0169-555X/$ – see front matter © 2013 Elsevier B.V. All rights reserved.
http://dx.doi.org/10.1016/j.geomorph.2013.04.022

Fig. 1. Reference map of the study area in Imperial County, California. An annotated Google Earth image of the study area showing the locations of the fumaroles discussed in this paper is shown in Fig. 2.

Table 1
Locations and descriptions of the major vent fields.

Name	Latitude	Longitude	~Size (m)	Comments
F1	N 33.2210	W 115.6036	25 × 50	Boiling hot, exposed, surroundings dry
F2	N 33.2184	W 115.6011	120 × 400	Boiling hot, exposed, surroundings dry
F3	N 33.2135	W115.5931	30 × 50	Hot, steaming, exposed, many salses, surroundings wet and muddy
F4	N 33.2150	W 115.5937	50 × 60	Partially exposed, many salses, a few gryphons, not steaming
F5	N33. 2122	W115.5951	100 × 100	Underwater, many vents flowing mud, not steaming
F3N	N 33.2141	W 115.5935		Possible vent field, under water, not steaming
F3S	N 33.2126	W115.5931		Possible vent field, under water, not steaming

The entire area in the bayou around F3 shows many vents and vent lineaments. F1, F2 & F3 are the only vents observed to be steaming hot.

magma produced the Salton Buttes, five late Quaternary rhyolitic volcanic necks near the southeastern end of the Salton Sea (Robinson et al., 1976; Newark et al., 1988).

The Salton Sea occupies the lowest part of the Salton Trough. It is a saline, eutrophic, endorheic rift lake (Dangermond, 2003; Hurlbert, 2008) that was created when a canal breach diverted the Colorado River into the Salton Trough in March 1905. Fresh water flowed north through the New River and Alamo River (Kennan, 1917). After the canal was repaired in Feb 1907, the high water level of −59 m MSL (−195 ft) decreased rapidly to around −76 m MSL (−250 ft) in 1917. Rain and runoff gradually raised the sea level, reaching a high of about −70 m MSL (−229 ft) in the mid 1980s, after which legislation resulted in a gradual lowering of the sea level that continues to this day (Lynch, 2011).

Where the Salton Sea overlaps the Salton Sea Geothermal Field, the interaction of rising gas and hot water with sediments has produced a number of hot, fumarolic gryphons and salses (LeConte, 1855; Veatch, 1860; Helgeson, 1968; Muffler and White, 1968; Sturz et al., 1992, 1997; Svensen et al., 2007; Lynch and Hudnut, 2008; Manga et al., 2009; Svensen et al., 2009; Rudolph and Manga, 2010; Onderdonk et

Fig. 2. Annotated Google Earth image of the fumaroles in our study area from Table 1. Mullet Island is upper left, the Davis–Schrimpf gryphons at lower right (DS). The evident NW-trending lineament of the geothermal features is suggestive of a fault, probably the Calipatria Fault (Lynch and Hudnut, 2008).

Table 2
Field observations, circumstances and general findings.

Date	Observer location	Activity and summary of findings	Water level
Various 2006	Ground	F1 & F2 covered by Salton Sea and venting steam clouds. Approximate locations measured by triangulation	−228 ft (−69.49 m)
8-Jun-07	Airboat	F1, F2, F3 covered with a few cm of water, some mud exposed. F2 hot and actively spitting mud, water and steam clouds. Locations of F1 and F2 measured using handheld GPS receiver (Lynch and Hudnut, 2008)	−228.9 (−69.77 m)
6-Apr-10	Aircraft	F2 exposed and showing surface mud flows, gryphons and salses (Tratt and Lynch, 2010). F1 & F2 found to be venting ammonia (Tratt et al., 2011). F1 below Salton Sea level	−231.7 (−70.62 m)
13-Aug-10	Aircraft	F2 exposed, showing changes in mud flow patterns. Gryphons and salses changed since April 2010. F1 below Salton Sea level	−231.9 (−70.68 m)
9-13 Nov 2010	Aircraft	USGS LiDAR imagery of Salton Sea shore (Dewberry, Inc., 2011)	−231.9 (−70.68 m)
18-Jan-11	Ground	F1 and F2 visited and photographed. F1 exposed, location measured using hand held GPS receiver	−231.6 (−70.59 m)
26-Jan-11	Ground	F1 and F2 visited and photographed. Samples taken for lab studies	−231.5 (−70.56 m)
28,29 Jul 2011	Aircraft	Low altitude imaging, location of F3 measured during flyover and verified using georegistered photographs. F3 found to be exposed, showing gryphons and salses. F5 discovered and located	−231.7 (−70.62 m)
15, 16 Set 2011	Ground	F1 and F2 visited and photographed. Sulfur vents found at F1 and F2. Samples taken for lab studies. Sediments surrounding F2 sampled for lab studies	−232 (−70.71 m)
12, 13 Oct 2011	Ground & aircraft	F1 and F2 visited and photographed. Water samples taken, accessible vent temperatures measured. Aerial measurements revealed precise locations of F3 & F4. Follow up examination of Google Earth imagery revealed F3N & F3S	−232.5 (−70.87 m)
12-Feb-12	Ground	Photos of F1 and F2. Water level was higher since the previous visit and the area was much wetter.	−231.9 (−70.68 m)
10-Sep-12	Ground	Photos of F1 and F2. Water level down and area much drier than previous visit.	−232.1 (−70.74 m)

Salton Sea level MSL, NGVD 1929, Westmoreland Gauge, USGS 10254005 http://waterdata.usgs.gov/nwis/dv?referred_module=sw&site_no=10254005.
Datum shift (NAVD 88 minus NGVD 29) = 0.663 m (2.175 ft). Original data measured in feet.

al., 2011). Much of the activity involves rising CO_2 produced by hydrothermal alteration of calcareous components of the Colorado River sediments (Muffler and White, 1969).

Since the Salton level began dropping in ~1983, a number of fumarole fields were exposed subaerially in extreme southeastern California (Fig. 1) for the first time since ~1945. The first emerged in ~2007 and others are still below water level or are being exposed as of this writing. These on-going events provided the motivation for this paper. Here was a unique opportunity to study the birth and evolution of gryphons and salses ab initio. The goal was to understand their physical development by monitoring them as they grew and matured over a seven year period.

Fig. 2 shows the locations of the newly-exposed fumaroles. We have named the most accessible of these F1 and F2 (Table 1). In 2011 we discovered several more vent fields from aerial photographs (F3, F4 and F5, Table 1), about which little is known because of their inaccessibility. None of these fields were studied by Helgeson (1968), Sturz et al. (1992, 1997), Svensen et al. (2007), Manga et al. (2009), Svensen et al. (2009), Rudolph and Manga (2010), and Onderdonk et al. (2011), whose subjects were the gryphons and salses at the Davis–Schrimpf field (DS).

The fumaroles at F2 were first reported in the literature in 1855 by LeConte, and later discussed by Veatch (1860) and Hanks (1882). Hanks gives their location as section 15, township 11 south, range 13 east, San Bernardino meridian, which exactly corresponds to the F1 and F2 fields, and excludes the Davis–Schrimpf field.

2. Material and methods

Photography was done using a Nikon D90 digital single lens reflex camera with an attached GP-1 GPS encoder for each image. Nadir and oblique aerial photographs were obtained from an altitude of 50–450 m AGL (Above Ground Level). During November 2010, a LiDAR (Light Detection and Ranging) survey of the Salton Sea shoreline and environs was

Fig. 3. Nadir-looking, aerial photo of the central part of F2 taken on April 6, 2010 (Tratt and Lynch, 2010). Note the large number of gryphons (dark, discrete ~circular structures) and the runoff of dark sediment brought to the surface by the gryphons.

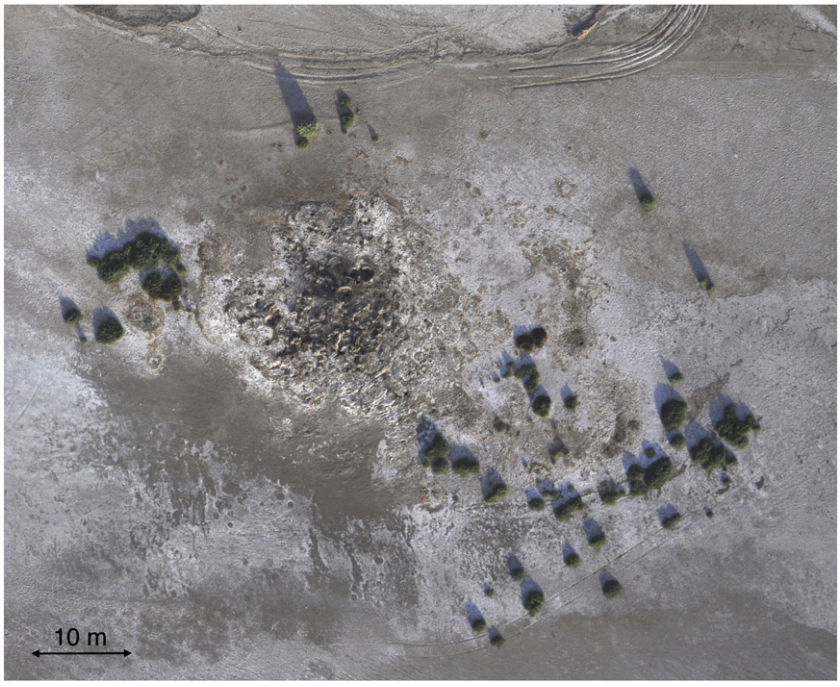

Fig. 4. Low sun elevation aerial photograph of F1. Note the shadows of the surrounding plants and the absence of long shadows in F1, indicative of its low topographic relief. F1 also shows a diffuse, light colored rind of surface evaporite deposits (July 28th, 2011).

carried out by Dewberry, Inc. (2011) from an elevation of 800 m AGL (nominal).

In situ measurements of mud and water temperatures were performed using a Robinair 43230 digital thermometer inserted into the sediments to a depth of 10 cm. Wet mud samples were collected from two locations at F1 and three at F2 in January and September 2011, and transported to the laboratory for immediate analysis. Samples were air dried (never heated) in order to remove moisture but minimize dehydration of hydrated phases. Laboratory studies were performed using a JEOL 6460LV scanning electron microscope (SEM) equipped with an Oxford INCA energy dispersive spectrometer (EDS). The EDS has a thin window and can detect elements with atomic masses as small as boron. They were prepared for SEM analysis by sonicating a small amount of material in a vial containing isopropanol. This was done in order to disaggregate any clusters of grains that may have formed during drying. This solution was then filtered through a 25-mm diameter, 0.3 micron filter and the dried filtrate was attached to a carbon stub and carbon coated to eliminate charging in the SEM. Additionally we employed an X-ray diffraction (XRD) using copper K alpha radiation and a PANalytical X'Pert Pro diffractometer equipped with an X'Celerator real time multistrip detector. Samples were mounted on a "zero background" plate, a quartz crystal cut at such an angle that it produces no X-ray reflections and very little background.

3. Observations and results

Table 2 contains summaries of findings from twelve field observations between 2006 and 2012.

3.1. Aerial photography

Based on historic imagery available in Google Earth, F2 was exposed sometime between Aug 2006 and Feb 2008. One of us (DKL) visited the area on an airboat on June 8th, 2007 and found the F2 region partially exposed. Owing to seasonal changes in Salton Sea water levels (Westmoreland Gauge), F1, F2 and F3 have probably experienced several episodes of submersion and exposure between 2006 and 2008. The first known detailed photograph of exposed F2 (Fig. 3) was taken on 6 April 2010 by D. Tratt (Tratt and Lynch, 2010). The photo showed extrusive mud flows, gryphons, salses and steaming vents. Surface mud flow patterns changed markedly between the two dates. Between Aug 2010 and Jan 2011 the water level had dropped enough to expose F1.

On July 28th & 29th, 2011 we completed a low altitude aerial survey using a nadir pointing Nikon D90 DSLR with an attached GP-1 encoder, and employing the techniques described by Lynch et al. (2010). Nadir-pointing aerial photos of F1, F2 and F3 are shown in Figs. 4, 5, and 6, respectively. Additionally, aerial pictures and videos were obtained on Oct 13th, 2011 from an Airborne XT 912 light-sport aircraft.

3.2. Geomorphology

3.2.1. Overall setting

F1 and F2 sit on a flat, horizontal, slightly elevated sand bar roughly 1000 m × 1200 m oriented with the long axis oriented ~N45E. Fig. 7 shows the results of a LiDAR imagery of the F2 region. At the time of the survey, the highest part of the F2 grade was less than 0.5 m above the Salton Sea water level and fell off gradually in all directions. Neither LiDAR nor field inspection revealed any evidence of tectonic features such as scarps, ridges or offset channels.

3.2.2. Fumarole field F2

F2 is by far the most extensive fumarole field in the region. Its surface represents the naturally exposed and desiccated Salton Sea floor. The original lake sediment of the sand bar is medium brown and soft, consisting of quartz and feldspar cemented by evaporites like gypsum, NaCl, calcite, anhydrite, etc., that overlaid very fine grained, dark gray mud (Tables 3 and 4).

Immediately surrounding F2 is a "rind" of lighter colored material 30–100 m wide that is rich in evaporite effluent from the gryphons (Figs. 4, 5). This region showed flow patterns indicative of aqueous material flowing radially away from the elevated gryphon field, primarily to the NE where the surface slope is largest. The flow patterns changed with each visit.

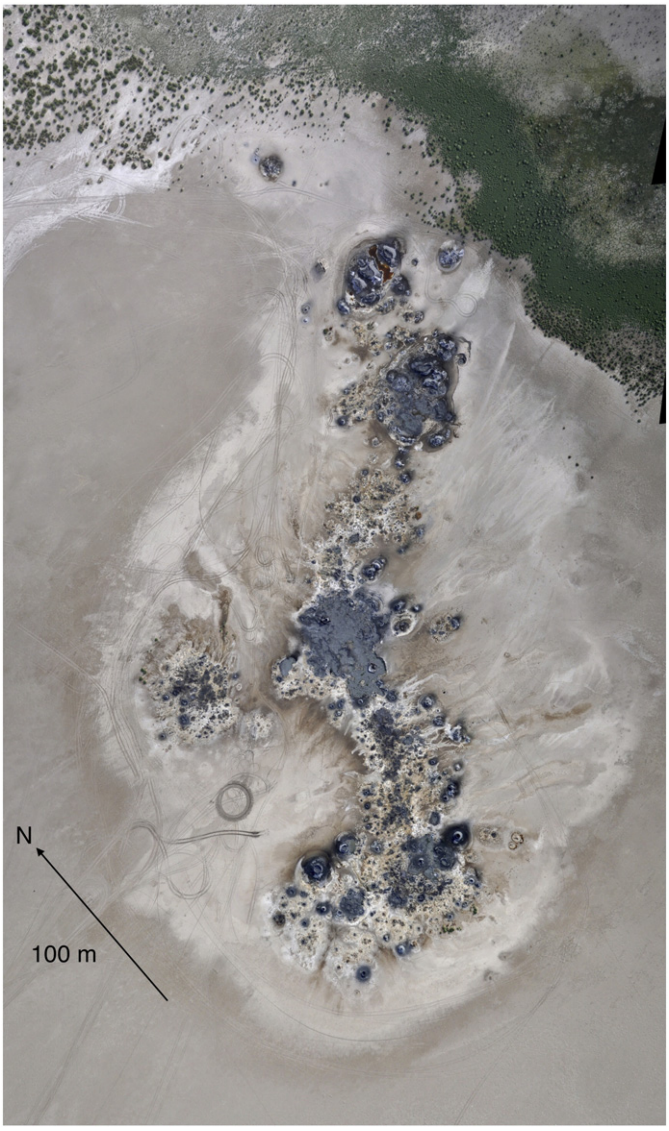

Fig. 5. Mosaic of three aerial photos of F2 showing the exposed seafloor sediment (beige), and the lighter colored evaporite rind surrounding the dark gray gryphons. A circular tire track from 4WD visitors is evident (July 29th, 2011).

Owing to the shallow water table, the region is muddy and wet, making walking difficult and in some cases impossible. As a result, few if any of the gryphons could be approached for hands-on examination. Near the gryphons, the ground is warm or hot to the touch. In many locations, hot mud (~100 °C) is only a few cm below the surface.

Sitting atop and inside the rind is the F2 fumarole field itself (Fig. 8). It is roughly 400 m by 120 m (~5 ha) and tends generally NE. F2 consisted of hundreds of gryphons and salses, and countless gas vents. Most were active, emitting hot mud (100 °C), and gas (mostly water vapor and CO_2) that immediately cooled to form water drop clouds ("steam clouds").

Gryphons ranged in height from a few cm to ~2 m. Their base diameters varied from a few cm to up to 10 m. Some were single structures, others were composed of several gryphons that grew and merged with other composites. As mud was extruded, many gryphons had merged to form complex, irregular cones with several spitting vents. The larger complexes showed the characteristic moats and ring scarps (Fig. 9), discussed in detail by Onderdonk et al. (2011). In many cases, mud flowed down the flanks and formed ropey, pahoehoe-like surfaces. There were also many mud pots and salses, usually showing peripheral collapse structures and ring scarps. The gryphons were composed of dark gray mud that dried to light gray. Emission from the vents included water, mud, CO_2 and in a few places H_2S and NH_3, as judged by smell (no gas sampling equipment was available). Using airborne infrared hyperspectral imagery, Tratt et al. (2011) reported strong ammonia emission from F1, F2 and F3 on four flights between March 2009 and August 2011. Ammonia venting appears to be persistent; it has been detected on every hyperspectral flight over the area.

In many ways, the gryphons' morphologies are analogous to those of igneous volcanoes. Consequently we have adopted the corresponding terminology. Gryphons showed a range of shapes including steep-sided "spatter cones", and "composite" gryphons. Their eruption mechanisms also appeared to be analogous to conventional volcanoes. Strombolian-like eruptions produced spatter cones. Effusive eruptions formed composite gryphons of mud extruded from the central and side vents that flowed down the flanks. Somma gryphons (small gryphons in salses atop larger gryphons) were common. Owing to possible temporal variations in the gas and water content of the mud, or differences in subsurface conduit properties, some gryphons showed both spatter cones and composite surfaces. Large gryphons of both types were usually surrounded by a depressed region filled with water (Fig. 9), a moat-like structure. LiDAR measurements (Fig. 7) revealed that the water levels were the same as the Salton Sea level. In every case, composite gryphons had less steep flank slopes than spatter cones.

Spatter cone gryphons were numerous, some exceeding 1.8 m in height. Isolated cones were more or less symmetric about the central vent. Those close together often merged and became asymmetric. (Fig. 10). The largest spatter cones were steep sided, some exceeding 45°. Smaller and presumably younger spatter cones have less steep flank slopes. Spatter cones had conical straight-sided flanks, or displayed nearly bell-shaped profiles. Explosive release of gas propelled viscous mud clasts from the vent that fell onto the flanks and welded to previous deposits to build up the gryphon. Some of the ejected mud clasts landed on the surrounding ground where a dark ejecta blanket was evident.

Spatter cone gryphons would seem to follow the same mechanism: relatively low amounts of water resulting in viscous mud, with gas released explosively and mud clasts being launched from the vent. Being somewhat sticky, the clasts weld to previous deposits, forming a rough outer surface to the spatter cone. Based on visual estimates of the maximum height attained by the ejecta, clast flight times and the dimensions of the gryphon (estimated by eye in the field), maximum eject velocities were less than 5 m/s. This value is consistent with the diameter of the ejecta blanket which for large gryphons (~1.5 m high) was typically 6–8 m across.

F2 contained hundreds of "mud towers", unusual gryphons in the form of slender vertical tubes with central vents emitting hot gas and relatively inviscid mud (Fig. 11a and b). They ranged in height from a few cm to over 0.5 m, and were between 3 and 20 cm wide. Isolated mud towers were the most common, but many were also formed inside or atop composite gryphons. To our knowledge these mud towers are unique to this fumarole field; we are unaware of similar structures being reported anywhere in the world.

Salses were common and most contained bubbling water and dark gray mud (Fig. 12). Their sizes ranged from a few cm to over 20 m. Many were circular; others were irregular in shape owing to merging with nearby mud pots. Most were steaming and a few were sufficiently wet and active that bursting bubbles threw mud clasts beyond their edges. At several places in F2 and especially near the NE end, there were quiescent salses with a distinctive red-brown color (Fig. 13), perhaps due to halophilic bacteria. Soft mud and hot water prevented direct sampling.

In September 2011, C. Schoneman of the US Fish and Wildlife Service (personal communication) reported what he believed to be a sulfur vent at F2. Subsequent inspection by the authors a few days later confirmed his observations, and further revealed dozens of such vents in F1 and F2 (Fig. 14). The vents were discrete and found

Fig. 6. Aerial photograph of fumarole field F3. The large amount of surrounding gray sediment-laden water suggests a net upward flux of mud (July 28th, 2011).

in groups on slightly elevated structures, some on gryphons, others being more or less isolated. They were typically a few cm across and with a periphery of yellow or greenish-yellow opaque, bladed or acicular sulfur crystals less than 2 mm long. In most cases the vents were expelling hot gas, some audibly.

Temperatures were measured at about a dozen locations around the periphery of F1 and F2 by inserting a calibrated (with ice and boiling water) digital thermometer into the sediments near sulfur vents to a depth of 10 cm. In all cases the temperatures were very high, 98–100 °C. The steam clouds emanating from fumarolic vents were a testament to the shallow depths of boiling water.

3.2.3. Fumarole field F1

F1 resides on the same flat, sandy bar as F2. It is about 650 m SE of Mullet Island and 400 m NW of F2. It was about 25 m by 50 m, is very wet, and had very few elevated structures, none higher than ~30 cm. (Fig. 15). Sulfur vents were common in September and October 2011. There are dozens of active salses, and many showed clear bubbling water, something almost completely absent from F2. Indeed, there must be significant differences in the underground plumbing properties between F1 and F2 to cause such different surface morphologies.

3.2.4. Fumarole field F3

F3 was surrounded by water and was inaccessible by foot. Aerial photography from July 29th, 2011 revealed it to be about 30 by 50 m, and composed of dozens of salses. F3's mud was dark gray and could be seen flowing into the bayou and coloring the water. In October 2011 we were able to make low altitude flights over the fumarole areas and observe F3 directly (Fig. 16). It is in a marshy area and other mud pots are evident, both above water level and below (Table 1).

3.3. Other vent fields in the area

During the July and Oct 2011 flights we observed several other vent fields and two more water-covered suspected fields (Fig. 2). Owing to thick brush, marshy water and muddy terrain, field access to these vents has not yet been achieved. F4 is a cool (nonsteaming) field of salses and a few gryphons located about 160 m NNW of F3. It is partially underwater and abuts a vegetation line at the shoreline (Fig. 17). F5 (Fig. 18) is located underwater about 220 m SW of F3 and shows evidence of many vents expelling mud into the bayou, though without steam clouds. Suspected vent fields F3N and F3S were identified from what appears to be mud being injected into the waters of the bayou (Fig. 19). Photographs from July and Oct 2011 reveal that vents in the bayou are injecting gray mud into the water. Some vents are clustered in large fields, others arranged in lineaments. Countless others occur as isolated vents.

3.4. Laboratory analysis

Laboratory analysis (Tables 3, 4) revealed that the main component of the mud was quartz (~60–80%). Gypsum, halite, calcite, dolomite and various minor feldspars were also common. Despite the variation in mud color, there was little if any difference in composition. Such a circumstance is probably due to variations in small amounts of very fine-grained material (like iron oxides) that acts as a pigment while having little influence on gross composition. Listed in Table 3 are the compositions of the mud taken from two locations in F1 and three in F2.

In addition to quartz, halite, calcite and dolomite, a number of common sulfate minerals were present: glauberite, bassinite, anhydrite, thenardite, and bloedite. Two unusual ammoniated sulfates were also found at several locations: boussingaultite $(NH_4)_2Mg(SO_4)_2 \cdot 6(H_2O)$ and lecontite $(NH_4,K)Na(SO_4) \cdot 2H_2O$. Boussingaultite is a rare sulfate mineral (Taylor, 1858; Larsen and Shannon, 1920; Winchell and Benoit, 1951; Anthony et al., 2003) that is known to sublime under fumarolic conditions. Ammonia NH_3 is abundant in Salton Sea sediments, originating from the decay of algae and agricultural runoff of ammonia-based fertilizers (Holdren and Montaño, 2002; Miller et al., 2005). Tratt et al. (2011) reported significant ammonia venting from F1, F2 and F3, probably the result of entrainment of ammonia by rising CO_2. Mullet Island

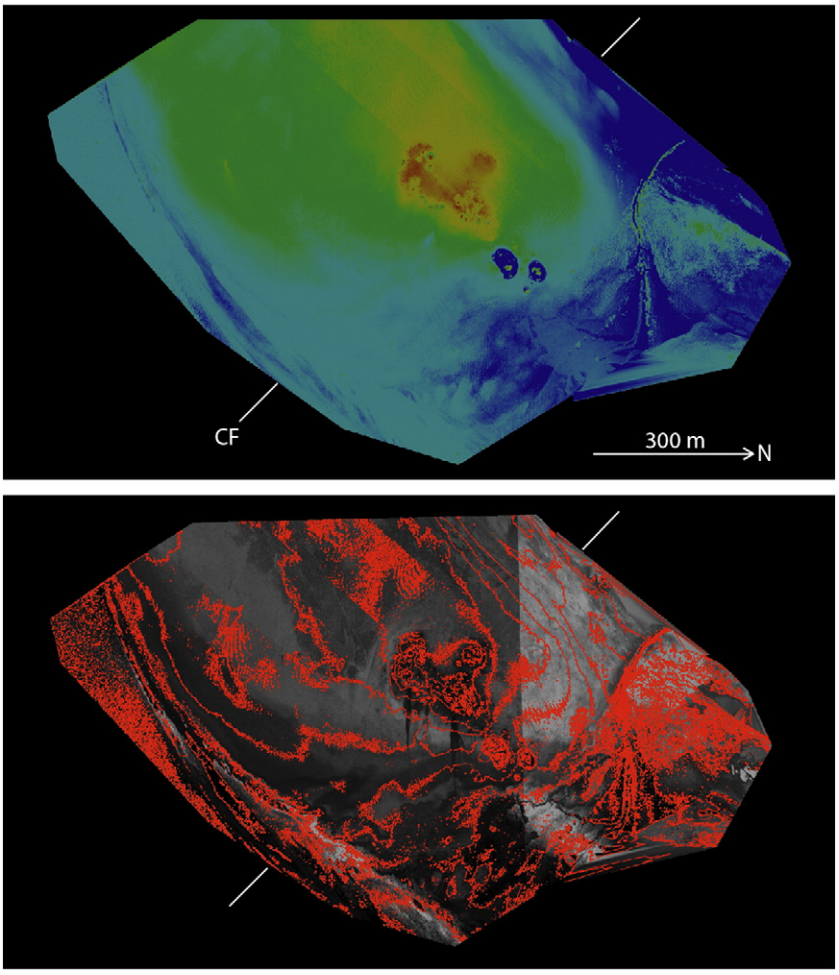

Fig. 7. Processed USGS LiDAR images of the F2 field from November 2010 (Dewberry, Inc., 2011). Upper: elevation. Scale: dark blue to red = 0.5 m. The sandbar containing F2 is very flat with virtually no significant topography except for the volcanoes and mud pots. Note that the moats around the prominent volcanoes are at the same level as the sea surface (dark blue). Lower: LiDAR return brightness (gray) with an overlay of elevation contours (red). Contour spacing is 10 cm. CF—approximate trace of the Calipatria fault. Neither LiDAR nor field inspection revealed any evidence of tectonic features such as scarps, ridges or offset channels. The small stream immediately NW of F2 appears to vary its location over time and shows no apparent geometrical relation to the axis of the putative Calipatria fault. The Salton Sea Level during the LiDAR survey was −70.7 m NGVD 29, or −78.3 m NAVD88.

also showed ammonia plumes, presumably from guano. Boussingaultite is also known to form in the absence of free ammonia (Pinch, 1978).

SEM pictures of the sulfur crystals revealed well-formed orthorhombic crystals with rounded cavities (Fig. 20). All of the SEM pictures of sulfur we obtained from F1 and F2 had similar crystallographic habits and morphologies. Laboratory XRD analysis revealed the sulfur to be primarily orthorhombic α-S_8 crystals.

3.5. Time evolution of F2 and environs

The formation and growth of gryphons were observed episodically for seven years (Table 2). We visited F2 on June 8th, 2007 when most of it was still beneath a few cm of water. At this time the Salton Sea water diluted the upwelling mud, making it watery and inviscid. As a result, the mud had little compressive strength and could not sustain significant vertical growth. Currents in the Salton Sea washed away

Table 3
Samples from September 2011.

Name	Setting	Composition
F2-1	Sulfur vent	Sulfur, quartz, calcite
F2-2	Sulfur vent	Sulfur, gypsum
F1-1	Sulfur vent	Sulfur, quartz
F2 background	33.2172–115.6028	Halite, quartz, glauberite $Na_2Ca(SO_4)_2$
f2 rind	33.2174–115.6026	Halite, quartz, gypsum, calcite

Table 4
Samples from October 2011.

Name	Location	Composition
S1-1	Salse S1 in F2 33.21731–115.60124	Gypsum, quartz, minor bassinite $2CaSO_4$ (H_2O) & halite
S1-2	"	Halite, gypsum, anhydrite $CaSO_4$, quartz
S1-3	"	Sulfur, minor quartz & gypsum
S1-4	"	Boussingaultite $(NH_4)_2Mg(SO_4)_2 \cdot 6(H_2O)$, thenardite $Na_2(SO_4)$, minor quartz & lecontite $(NH_4,K)Na(SO_4) \cdot 2(H_2O)$
S1-5	"	Sulfur, minor quartz & gypsum
S5-1	Salse S5 in F2 33.21954–115.59950	Quartz, halite, calcite
S5-2	Salse S5 33.21954–115.59950	Quartz, halite, minor calcite & bloedite $Na_2Mg(SO_4)_2 \cdot 4(H_2O)$
S vent rind	Sulfur vent in F1	Gypsum, quartz, minor bassinite & halite
S vent background	Near sulfur vent in F1	Quartz, glauberite $Na_2Ca(SO_4)_2$, halite, minor calcite & dolomite

Fig. 8. View of F2 looking southwest. Foreground gryphon is about 1.4 m high (Jan 18th, 2011).

newly emergent mud, thereby further preventing any upward growth. We also visited the areas of F1 and F3 when they were still under water and neither of them showed steam clouds. Presuming that they were hot in 2007, the absence of steam clouds suggests that the hot gas was cooled and/or absorbed by the overlying water. It is therefore possible that F5, F3N, F3S and perhaps others will begin to show steam clouds when the water level has dropped enough.

After exposure, the fumarole fields evolved rapidly. Between April and Aug 2010, the surface coloration and mud flow patterns showed significant changes (Figs. 2, 3). Even between Jan 18th and 26th, 2011, there were marked visual alterations in F1, notably the amount of algae, and the color and shape of surface deposits. Pictures taken in 2011 documented marked growth of gryphons and salses. The evident trend was to larger, more massive gryphons and larger salses (Fig. 21). Such development suggests that there was a net upward flux of mud, rather than continuous recycling of mud like what seems to be happening at DS (Onderdonk et al., 2011). Indeed, recent plant growth in the immediate vicinity of the fumaroles – especially evident at F1 – is compelling evidence that water and mud are being raised to the surface. Owing to the impossibility of directly approaching and measuring F2's gryphons, we cannot quantify the amount of growth in most cases.

We did not notice sulfur vents in F1 and F2 in January 2011, although upon reviewing our photographs, a small number might have been present. In view of the large number of such vents observed in September 2011, it is clear is that a great many of them formed during the eight month period.

Seasonal variations in water level from rainfall and government-mandated water management will raise and lower the water table, resulting in occasional “rehydration” of the fumarole fields. One such episode was observed at F2 between Oct 2011 when the water table was low and the surface relatively dry, and Feb 2012 when the water level was up and the area was much wetter. Many of the gryphons had decreased in height, presumably the result of water infiltrating the mud and causing it to loose compressional strength and collapse or slump. Several previously isolated salses (e.g. S6, Appendix I) had ceased to exist as individual structures, having become incorporated into adjacent pools whose horizontal extent grew as the water level rose.

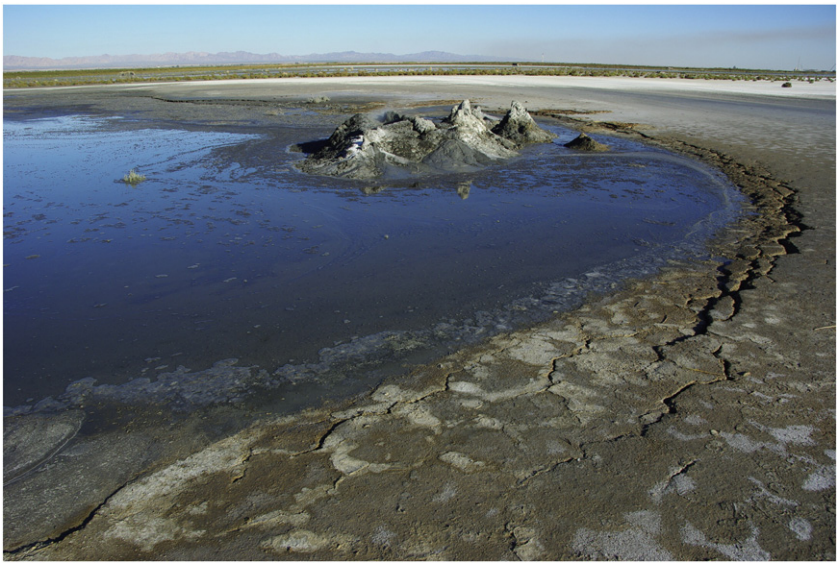

Fig. 9. Composite gryphon complex showing a ring scarp on the periphery of the moat. This is the southeastern part of the “village” (Appendix Fig. A1). Volcanoes are about 1 m high. View is to the north (Jan 18th, 2011).

Fig. 10. Spatter cone G3 at F2, average flank inclination 62°. Note the steaming central vent and rough exterior due to welded mud clasts. View is to the northwest toward Mullet Island, upper left. (Sept 15th, 2011). Also note the dark peripheral ejecta blanket from expelled mud clasts.

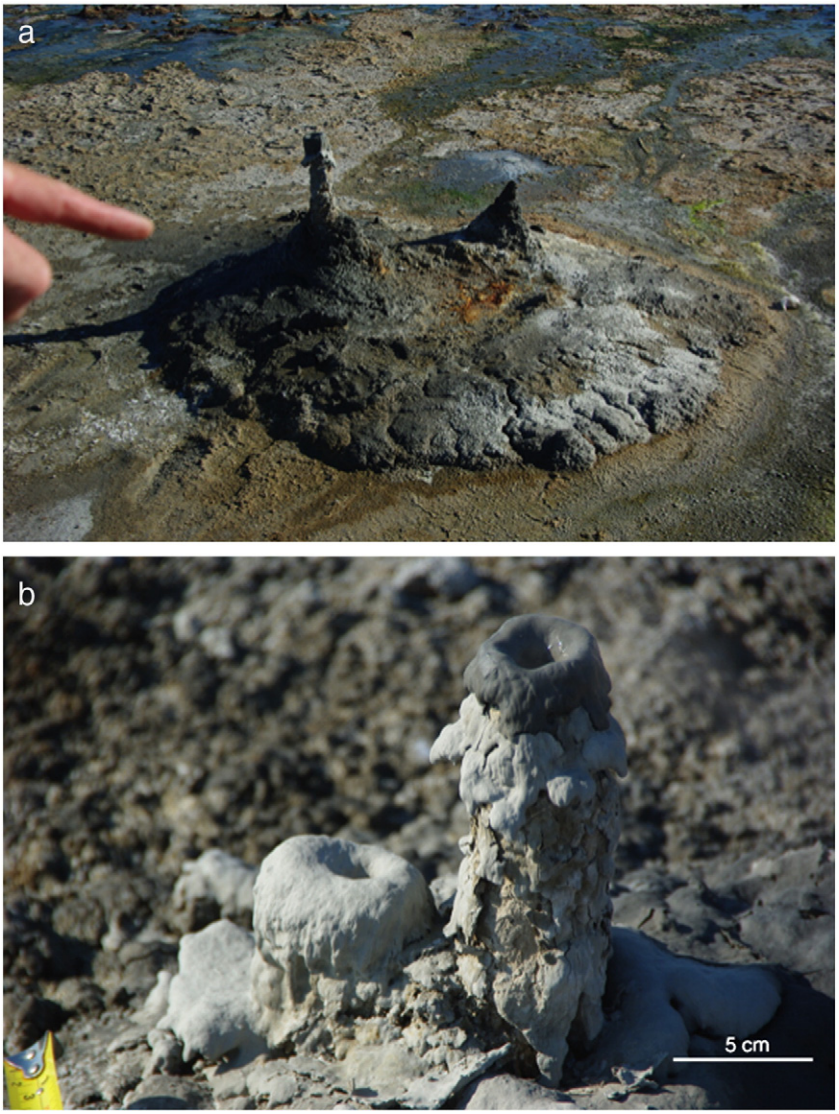

Fig. 11. (a) Mud tower about 30 cm tall. A week later the left tower had changed considerably (photo taken 18 Jan, 2011). (b) Gryphon G13 (Table A1). The morphology of this mud tower matches the description given by Veatch (1860) in 1857 (photo taken Sept 16th, 2011).

Fig. 12. Large mud pot S6 (Table A1) ~7 m across, showing ring scarps and collapsed walls. Some composite gryphons are immediately behind the mud pot (Sept 15th, 2011).

In September 2012 when the area had become drier, S6 had once again become an isolated mud pot.

4. Interpretation and discussion

The sand bar where F1 and F2 are located appears to be part of the natural Salton Sea floor that has probably been slightly modified by sediments entrained in water carried upward by rising CO_2. As the sediments settled, they accumulated and raised the sea floor, producing the slightly elevated sand bar. After subaerial exposure, continuing extrusion of mud and subsequent gravitational flow away from the sources further elevated the bar. The slight elevation of the bar suggests that there was a net upward mass transport of subsurface material. It is certainly possible, however, that the elevated bar is a natural consequence of delta development by the Alamo river.

We have no way of knowing if the rinds were present before the fumaroles were exposed. Assuming that water in the extruded mud contained dissolved minerals, it might have been dissolved and/or swept away by currents in the Salton Sea prior to surface exposure. From its fresh appearance in comparison to the rind at DS, we surmise that it is a relatively recent formation, probably deposited after the Salton Sea level dropped below the area permanently.

The absence of any tectonic features or lineaments in the fumarole fields that align or correlate with known faults in the area is not surprising. No surface rupturing earthquakes have occurred in the few years since F2 has been exposed. Even if such features had been produced in the Salton Sea sediments, currents in the sea would have eroded them and rendered the area essentially flat.

The main difference between F1 and F2 is that F1 contains essentially no gryphons. This may suggest that there are some sources of water or underground conduits that proceed largely through rock to the surface, entraining little or no mud. It might further explain why F1's structures show little vertical growth. The grade at F1 is about 20 cm lower than at F2, and F1 is closer to the Salton Sea water table, so any mud would probably be too inviscid to support significant vertical growth.

Structures similar to the mud towers we observed were reported at the same location in 1857 by Veatch (1860) who described them as "…a miniature grove of slender stalagmitic arborescent concretions of the same substance [mud]. They were from half an inch to

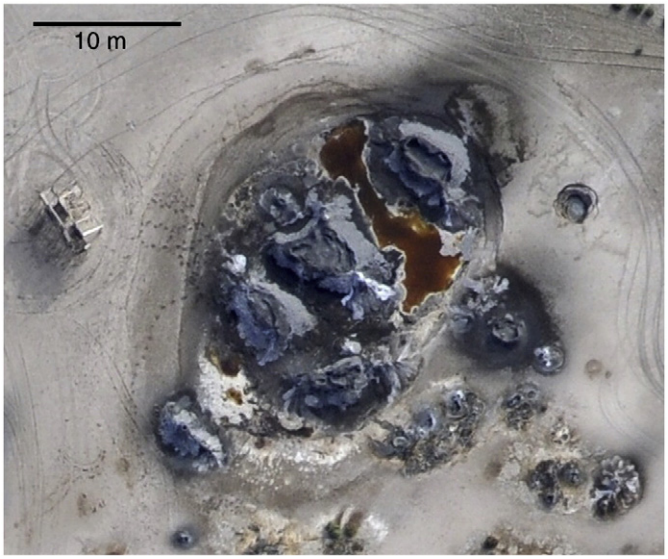

Fig. 13. Nadir-looking aerial photo of the G16 complex showing a quiescent, undrained pool with reddish suspended sediments believed to be halophilic bacteria. Salse S5 (Table A1) is the isolated structure at the right. The rectangular wooden structure at the left is a duck hunting blind (July 29th 2011).

Fig. 14. Close-up view of an active vent at F1 with a ring of small sulfur crystals (Sept 16th, 2011).

Fig. 15. F1 is a wet, hot fumarole field with many short structures and essentially no gryphons. Most of the salses show clear, bubbling water and almost no mud. The bottom width of the picture is about 5 m, and the truck in background gives a sense of scale. Temperatures measured at about a dozen locations around the edge of F1 during Oct 2011 were ~100 °C (Jan 18th, 2011).

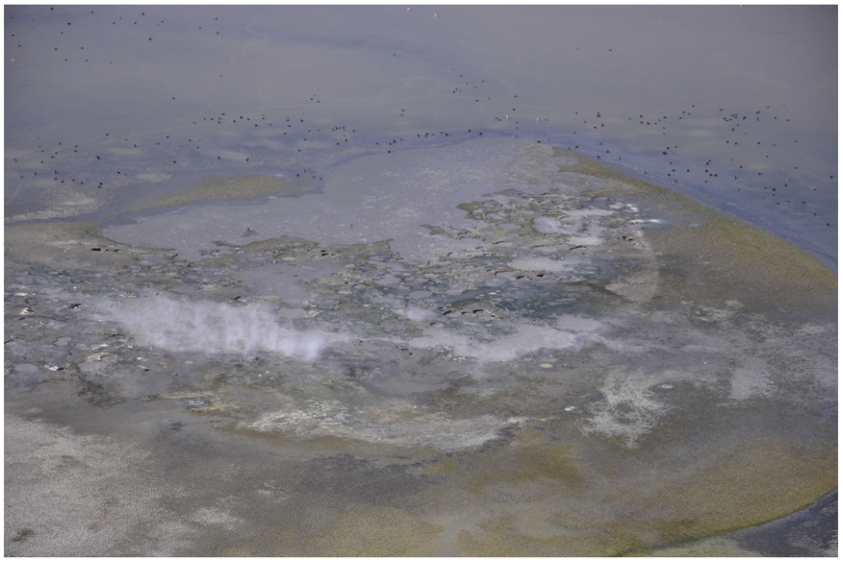

Fig. 16. Oblique aerial photograph of F3. F3 consists of hundreds of salses, many of them steaming hot. Few if any gryphons were evident. Image is about 50 m wide at the center. The numerous small dark spots are birds (13 Oct 2011).

Fig. 17. Vent field F4. No steam clouds were observed emanating from F4. Note that part of the field was still underwater. Duck blind at lower left is about 2 m wide. Width of this picture is approximately 100 m at the center (13 Oct 2011).

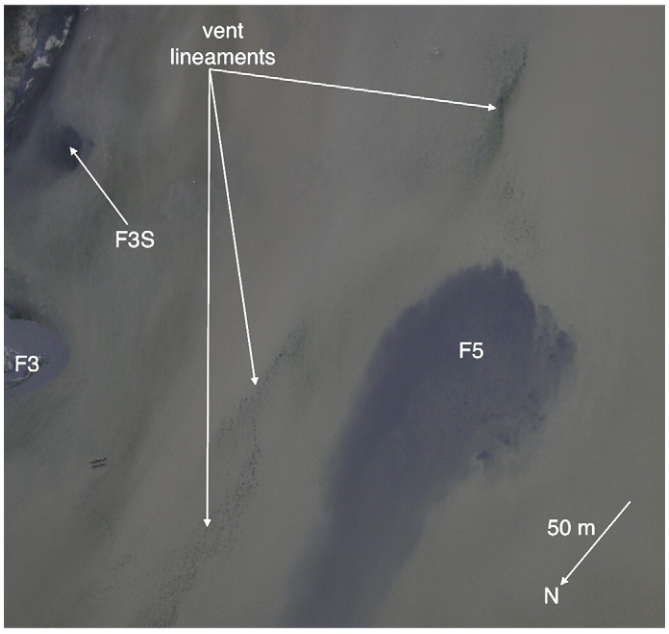

Fig. 18. Vent field F5 showing mud injected into the water and carried northward by currents. Some discrete vents can be seen on the west side of F5. Also shown are vent lineaments, F3S and F3. A close examination of the photo shows many discrete vents dotting the field of view (July 29th 2011).

one and one half inches in diameter, and from four to six inches in height…. Some were hollow, and delicate jets of steam issued from their summits, and this seemed to explain the mode of their formation. Some were not hollow throughout, being closed at the summit, but when detached from their base, a small orifice in the center suffered hot steam to pass….” From this description and our observations of what seem to be identical structures, we infer that mud tower production at F2 has been active for over 150 years whenever the surface was not covered by water.

A number of common sulfate minerals were found in and around the fumaroles, something not unexpected in view of the abundant sulfur vents. The presence of ammoniated sulfates such as boussingaultite and lecontite, however, is highly unusual in fumaroles. Fertilizer run off and bacterial activity in the eutrophic waters of the undrained Salton Sea have caused high levels of ammonia to accumulate in the water and

Fig. 20. SEM photographs of sulfur crystals from F1 showed them to be well formed with small spherical cavities.

lake bottom sediments (Holdren and Montaño, 2002). Ammonia is highly soluble in water and the aqueous environment affords an opportune setting for sulfur–ammonia chemistry.

The relatively sudden appearance or rapid increase in the number of sulfur vents between January and September 2011 could mean one of two things: 1) there was a fundamental change in the subsurface plumbing, chemistry or both, or 2) sulfur vent development is a normal occurrence as gryphons and salses develop after emerging from the water. Sulfur can form in fumarolic environments by several chemical pathways. The most common are water-catalyzed reactions $H_2S + 2SO_2 \rightarrow H_2SO_4 + 2S$, and water catalyzed oxidation of H_2S via $2H_2S + O_2 \rightarrow 2H_2O + 2S$ (Wang et al., 2008). In view of the aqueous environment of F1 and F2, and the rapid thermodynamic gradients at the mouth of a vent where atmospheric oxygen can mix with venting gas, the latter reaction would seem to be the most likely formation mechanism for the native sulfur observed. Hanks (1882) reported a “solfataric opening” and “several small cones, three or four feet high, from the top or summits of which issued sulfurous, carbonic and hydrosulfuric acid gasses, with a low incessant hiss.”

In view of the close proximity of F3, F3N, F3S, F4, F5 and the multitude of discrete vents (Figs. 17, 19), it seems likely that the entire

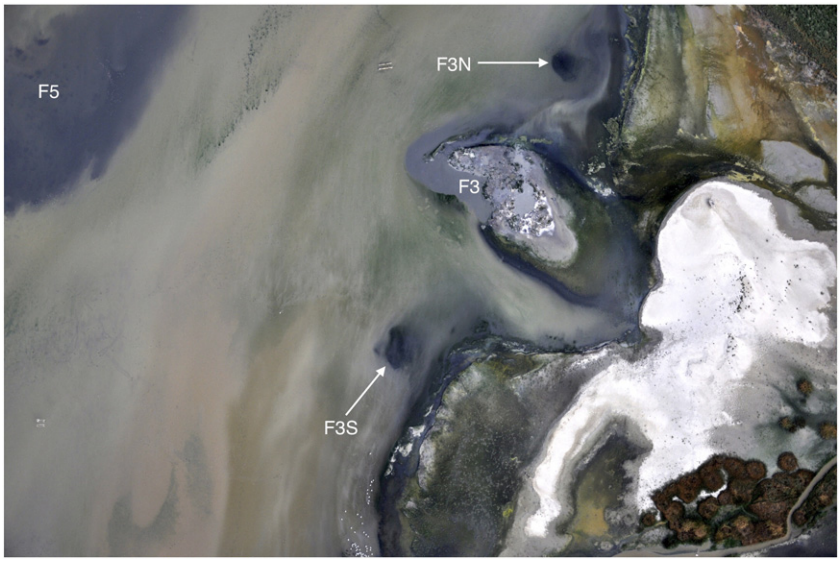

Fig. 19. Locations of F3, F3N, F3S and F5. Note also lineaments of discrete vents (upper left, right of F5) and complexity of the surface in the area (July 29th, 2011).

Fig. 21. Example of gryphon growth between Jan and Oct 2011. Here gryphon G16A (Table A1) grew vertically by about a 1 m. In Oct 2011 it was still in the spatter cone stage of development and growing. The wooden structure in the background is a duck blind. View looking NW toward Mullet Island. Steam clouds from F1 can be seen at the extreme left.

area is one large vent field (including F1 and F2). Our naming conventions may prove to be too simple or insufficiently descriptive, especially in view of the changing water levels and consequent changes in morphology of the geothermal features.

As the Salton Sea level decreases further, we expect the fumarole fields to grow dryer and eventually to reach a stasis where little or no water is brought to the surface. Ultimately, they will become desiccated vents, as those at DS are well on their way to becoming. During this time, the secular decrease in Salton Sea level will expose more and more fumaroles and vents and the morphological evolution will continue.

5. Model of gryphon evolution

Based on observations at F2 and F3 and the Davis–Schrimpf fields, we believe that gryphons near the Salton Sea developed progressively through several stages as the water table drops, the above-grade vent narrows, and the entrained mud becomes more viscous. This development is sketched in Fig. 22 and outlined it below.

Stage 1 Water covers the gas vent. The morphological expression of the seep on the sea bottom is only a conical depression in the sea floor. Many of these have been observed with SONAR in the Salton Sea (D. Brothers, 2010, personal communication).

Stage 2 As the water level reaches the sea floor, a salse appears, a shallow circular basin of bubbling, muddy water. Water lofted from the salse remains on the surface or runs back into the salse. There is little or no vertical development.

Stage 3 As the water table drops, muddy water in the salse thickens and the first mud clasts are ejected. These begin to accumulate on the periphery of the salse and form an elevated ring, the earliest stage of spatter cone development. The mud clasts have sufficient compressive strength to retain some vertical thickness upon landing. The spatter cone develops a rough, scaly outer surface as successive mud clasts weld to each other. Mud level in the vent is at or slightly below grade and near the level of the water table.

Stage 4 Water table drops below grade and mud thickens, becoming fairly viscous. Spatter cone develops with steep sides as ejected mud clasts accumulate. Mud level in the narrowing vent is above grade and above water table.

Stage 5 Rising mud is too viscous for significant ejection to occur. It is pushed upward by rising gas and reaches the top of the gryphon's vent. Mud begins to flow down the flanks and cover the rough spatter cone surface. This is a transitional stage and may be relatively short-lived.

Stage 6 Mud flows from the narrow central vent and completely covers the spatter cone, hiding all evidence of its rough outer surface. The gryphon's surface is now relatively smooth, with successive flows broadening the gryphon and covering earlier effusive flows. With a low water level and thick mud, the resulting composite gryphon is the end stage of gryphon development. Ultimately, the central vent may close completely, rendering the gryphon extinct and subject to weathering and disintegration.

The sequence outlined above is based on observations of hundreds of gryphons and salses in the Salton Sea fields. Every stage has been observed many times, and no other type of gryphon was seen. The most telling stage of development (stage 5) has been observed where effusive flow is observed at the top of a spatter cone. In no case was a spatter

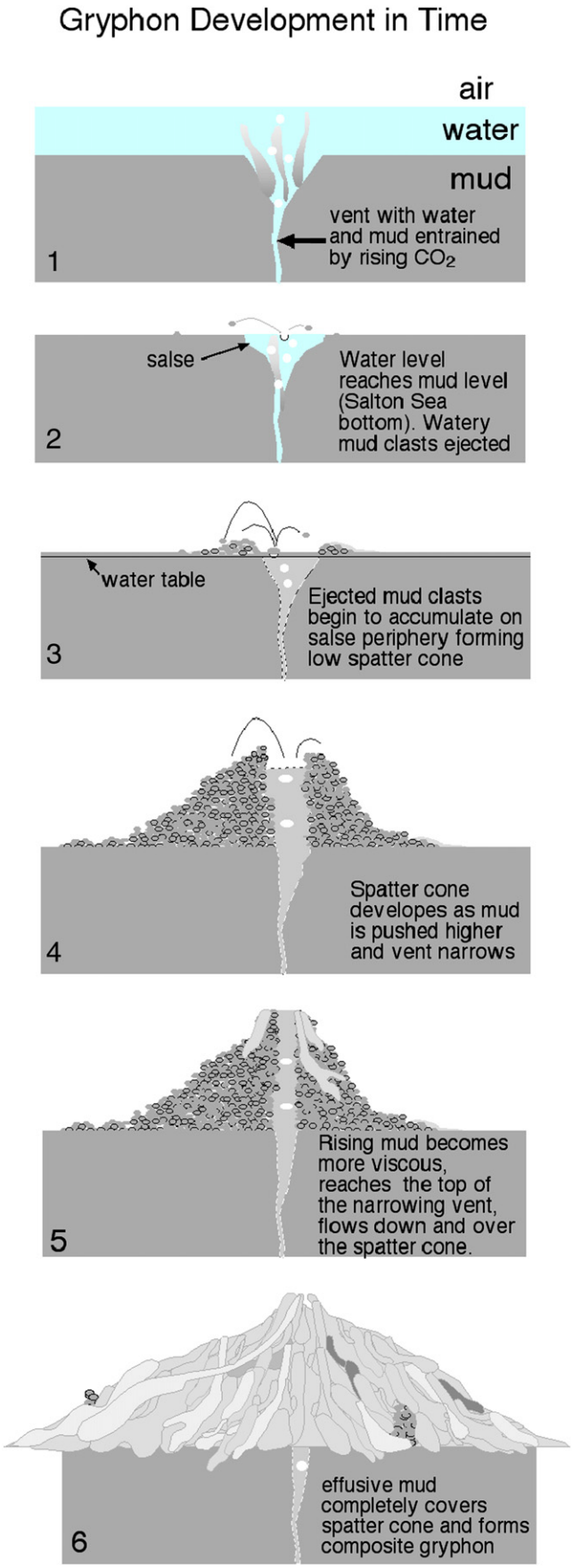

cone ever observed atop an effusive composite gryphon. According to our model, this could happen if the water level increases, thereby lowering the mud viscosity.

The presence of gryphons at F2 in every level of development is almost certainly a result of different gas/water/mud ratios. Although the development we have outlined is for a steadily lowering water table level, it appears that different locations can produce gryphons at different stages within the same fumarole field. Some gryphons may never evolve to stage 6; the underground plumbing may pinch off and render the gryphon extinct. Alternatively, the mud/water ratio may change, as it apparently did at Sulfur Hill (SH in Table A1), which is presently just emitting gas, its mud growth having stopped some time ago. Finally, not all salses will become gryphons; if the vent is particularly rich in water and poor in sediment, it can remain relatively unchanged. Indeed, Onderdonk et al. (2011) has noted the persistence of several salses at DS over many years.

As the Salton Sea level drops, there will be a good opportunity to observe and track gryphons at different stages of their growth. As of October 2011, F2 various gryphons were at stages 1–6, while those at F3 are at stages 1 and 2. Virtually all of the gryphons at DS are composite and in stage 6, where they have been for many years.

It is not clear how evolution would proceed if the water table rises. In situ observations of F2 in Feb 2012 when the water table was higher showed significant decrease in gryphon heights. Also, some of the larger salses (e.g. S6) had been annexed into the larger field and were no longer distinct, isolated features.

The simple model we have proposed is based on a single parameter: subsurface water level. It seems likely that other factors besides water level can influence gryphon evolution, such as mud viscosity, mud/gas ratio, vent width, recent rain fall, earthquakes, etc. The photographs presented here (and many not published) document a trend toward taller gryphons in the dry season, shorter ones after rain or when the Salton Sea level is higher.

6. Comparison of F2 and Davis–Schrimpf (DS) fields

Though presumably of similar origin, there are significant differences between the F2 field and the DS field, some of which may be due to their evolutionary stages and setting relative to the different water table levels. Based on the LiDAR data, surface elevation at DS is approximately 1.3 m above surface elevation at F2. F2 is much larger than DS, covering about 5 ha while DS covers roughly 1.4 ha. F2's evaporite rind is fresh and clearly evident; DS's rind is less pronounced, perhaps because it is much older and has been subject to aeolian modification and visitor traffic. Most of F2's gryphons are hotter (~100 °C) than those at DS (max temp 69 °C, Onderdonk et al., 2011). All of the gryphons at DS are of the composite variety with mud flowing from central or side vents and showing no spatter cones. F2 is wet year round, while DS dries out in the summer. Large composite gryphons at both sites had depressions encircling them. Many salses and mud pots at DS contained brown mud, while virtually none at F2 had brown mud. After September 2011 but not before January 2011, sulfur vents were common at F1 and F2, but none have been seen by the authors at the DS. However, a referee for this paper reported a single sulfur vent at DS.

Both fields have sulfate deposits. Surface sediment samples from F1 and F2 contained native sulfur from vents, many common sulfate minerals and two unusual ammoniated sulfates: boussingaultite and lecontite. DS does not show native sulfur, though Mazzini et al. (2011)

Fig. 22. The development of gryphons in the Salton Sea areas seems to follow a regular pattern that correlates with water table level. The end stage – if reached – is extinct, effusive (composite) volcanoes whose surface consists of dried mud that originally emanated from a central or side vents. After activity has ceased, the gryphons erode due to rain and aeolian processes.

Table A1
F2 major accessible structures, 12–13 Oct 2011.

Name	Lat N 33	Long E 115	Description (height above grade cm) G = gryphon, S = Salse or Seep, SC = spatter cone, C = composite (effusive), C/SC = C on top of SC
SH	0.21744	0.60237	Sulfur Hill, brownish gryphon, many hot sulfur vents, (75)
G1	0.21733	0.60226	SC gray ~12 m SW of SH, (44)
G2	0.21731	0.60207	SC gray ~21 m E of G1 (104)
G3	0.21729	0.60201	SC gray ~7 m E of G2, brown with recent mud flow from summit, sulfur vents on NW summit (118)
G4	0.21734	0.60238	Brown ~2 m wide, sulfur vent, most SW feature of F2 (~20)
G5	0.21739	0.6021	SC gray (89)
G6	0.21729	0.60177	SC gray (~30) with smaller SC ~1.5 m SW and sulfur vent ~1 m further W
G7	0.21728	0.6017	C/SC complex with mud towers on summits, moat (~50)
G8			SC 2 m S of G7
S1	0.21731	0.60124	Low seep, sulfate deposit rings (five samples)
S2			Low seep, sulfate deposit rings
G9	0.21746	0.60145	Big gray SC and moat (157) location approximate
G10	0.21787	0.60222	Big gray SC with partial moat and effusive-looking perimeter (131)
S3	0.21766	0.60247	Wet gray mud bubbles
S4	0.2178	0.60238	Wet gray mud bubbles, hissing
G11	0.21784	0.60232	Low SC gray (~25)
G12	0.21784	0.60195	SC with partial moat (85)
G13	0.22003	0.59957	Small C/SC (~35) with tall steaming mud tower (20 cm) and wet dark brown vent area
G14	0.22022	0.59968	C/SC complex, hissing (~80) many short mud towers
G15	0.22032	0.59978	Small gray SC mud pot (~40 cm), few m NW of G14
G16			Large complex of gryphons with large depression and reddish yellow water. Panorama
G16A			SC & C (149) inaccessible
G16B			SC & C (153) inaccessible
G16C			(119) inaccessible
G16D			(101) inaccessible
G16E			(112) inaccessible
G17	0.2195	0.59939	Isolated composite complex with partial moat (134)
S5	0.21954	0.5995	Large mud pot, oil seepage on N wall?
G18	0.21954	0.5996	Line of 3 gryphons and two seeps
G18A			C/SC (64) NW most gryphon on SW edge of G16 pool
G18B			SC (90)
G18C			C/SC (43)
S6	0.21903	0.59968	Large mud pot on E side of "village" Largest pot in F2. Incised by "village" ring scarp
G19	0.21763	0.60132	C gray complex with red water moat and ejecta blanket (85)
G20			SC 2 m W of G19
G21	0.21778	0.60105	three C gryphons
G22	0.21788	0.60107	C complex
G23	0.21794	0.60107	C & SC with moat (118)
D	0.21796	0.60100	Small quiet pot, good fiducial
G24	0.21817	0.60066	C complex with moat and attached salse, 1 SC
G25	0.21827	0.60088	C complex with mud towers
G26	0.21831	0.60078	C (78)
G27	0.21842	0.60082	C & SC (110)
G28	0.21855	0.60078	5 gryphons, E & SC, red water and ring scarp (121)
G29	0.21860	0.60060	Mud tower on top (111)
G30	0.21858	0.60044	C & SC (83)
G31	0.21878	0.60033	C/SC moat, ejecta blanket (54)
G32	0.21884	0.60028	C/SC (114)
G33	0.21882	0.60003	C/SC on SW edge of the "village" (131)
G34			SC in the village, inaccessible (158)
G40	0.21918	0.59963	C/SC (125)
G41	0.21933	0.59969	C/SC (71)
G42	0.21935	0.60027	C/SC with moat (61)
G43	0.21922	0.60039	SC gray (113)
G44	0.21896	0.60045	C/SC brown, gray mud tower on top, moat
G45	0.21861	0.60164	SC on edge of large pool (82)
G46	0.21853	0.60167	Low SC near edge of pool, just SW of G45
G47	0.21869	0.6018	C/SC in F2 North with a mud tower

found sulfate deposits of bloedite $Na_2Mg(SO_4)_2 \cdot 4(H_2O)$, and tamarugite $NaAl(SO_4)_2 \cdot 6(H_2O)$.

The structures at F1 and F2 are highly variable, and seem to be in a formative stage. Between January and October of 2011 they showed growth; most gryphons were taller, more massive and more complex than earlier. Most salses were larger and seemed to be expanding their diameters by wall collapse. Even the amount of algae and standing water at F1 changed between Jan 18th and Jan 26th, 2011, an eight-day period. The presence of inactive or dormant gryphons and salses at F2 observed in Sep & Oct 2011 is a testament to changes on the time scale of months to years. In contrast, measurements by Onderdonk et al. (2011) suggest that the DS field is in a steady state; there is little in the way of secular evolution of the gryphons and salses, leading them to the conclusion that the underground plumbing is stable and largely invariant over a 28 month period.

7. Tectonic implications

The locations of the Davis–Schrimpf field, F1, F2, F3 and Mullet Island fall on or cluster along a straight line (Fig. 2). We interpret this to be an indication of a fault. This lineament is probably the Calipatria fault, a feature previously discussed by Lynch and Hudnut (2008). This and other putative faults in the area strike N45W, more or less parallel to the San Andreas and Imperial faults. The Salton Buttes – clearly volcanic in origin and therefore likely to originate at a spreading center – fall along a curved arc that strikes ~N25E.

8. Summary and conclusions

Preliminary results are presented on fumarole fields that have recently been exposed by the dropping Salton Sea level between 2006 and 2011. The interaction between mud, water and gas in a desert environment, coupled with a high geothermal gradient has produced large variety of structures and phenomenology, including unusual chemistry and mineralogy. This work began before any gryphons at F1, F2, F3 and F4 were present and ended during an intermediate development stage, before most of them reached a steady state configuration like the mature gryphons and salses at the Davis–Schrimpf field. Of particular interest are the large number of spatter cones and the relatively sudden appearance of sulfur vents in 2011.

The work reported here is only a first look at the fumaroles, and many questions remain. Besides issues of dynamics, chemistry and hydrology, it would be useful to study emerging fumatoles in other parts of the world to see if the model set forth here is applicable there. As the Salton Sea water level continues to drop as it surely will (Quantification Settlement Agreement, 2003), how will the gryphons and salses change? With known vent fields still under water, we are presently in a good position to monitor them and watch gryphon development. Such observations would tell us more about how gryphons are formed and help refine the model set forth in this paper.

Acknowledgments

We thank Christian Schoneman of the US Fish and Wildlife Service for logistic support on various occasions. We are indebted to Brad Busch for expert piloting and to John R. Bayless of First Point Scientific for assistance during the July 2011 imaging flights. Howard Hall of Howard Hall Productions rendered valuable service in obtaining the October 2011 aerial photographs. Lee Case of the USGS provided the Dewberry LiDAR data. David Dearborn helped in locating the inaccessible fumaroles by developing photogrammetry software for overlaying geographic coordinates onto the aerial images. We are grateful to M. Bonini, Daniel Brothers and Katherine Scharer for helpful comments on early drafts of this paper. This work was supported in part by the Southern California Earthquake Center (SCEC).

Appendix I. Partial catalog of gryphons and salses at F2 (Oct 2011)

Figs. A1 and A2 show annotated images of the northeast and southwest portions of F2 field, respectively. The two images have the same scale and slightly overlap. Table A1 presents the precise

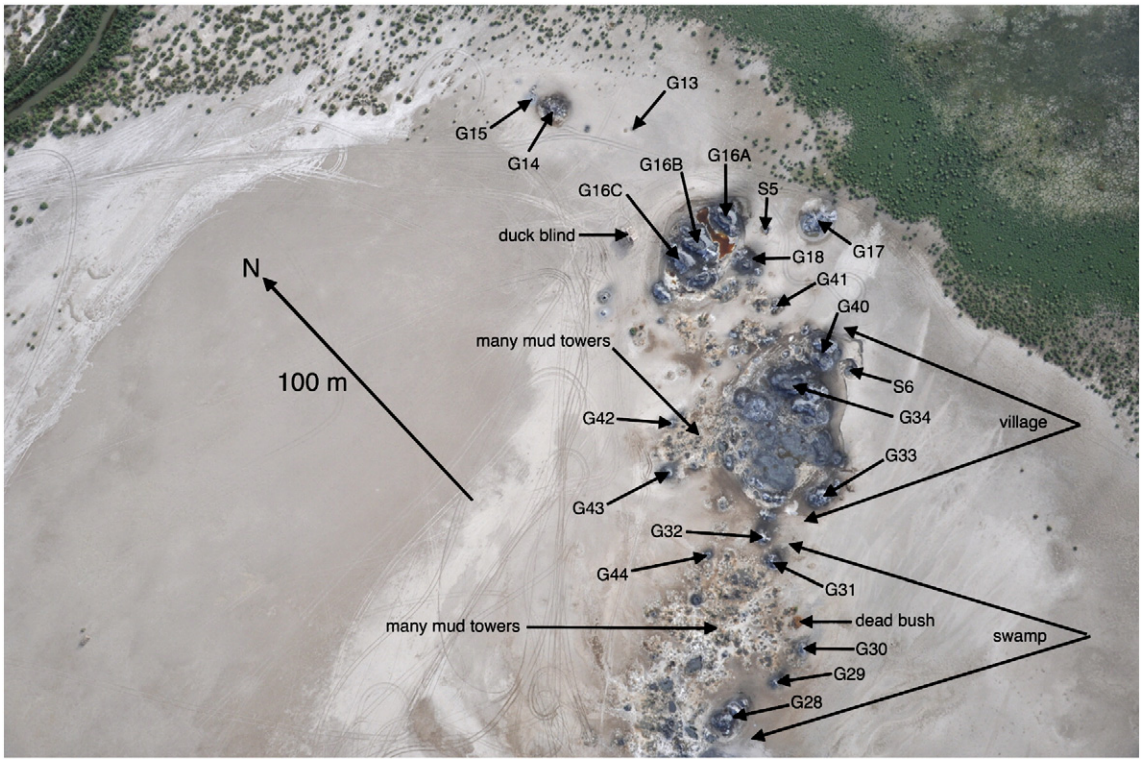

Fig. A1. F2, northeast section, annotated to identify gryphons, sales and regions with common geomorphology.

location of the indicated features along with information about each. Owing to the inaccessibility of most of the gryphons and time constraints in the field, we were only able to map those on the periphery of F2.

F2 contains a number of smaller regions that contain similar morphological features. Presumably the differences between them are related to locally-grouped variations in the subsurface conduits, mud availability and water flux. For convenience we have labeled these regions with a pair of diverging arrows in Figs. A1 and A2. The most active vents are in the north side of the "pond" (Fig. A2). Sulfur vents are found in many places but in Sept and Oct 2011, most are found on the southwest part of F2 in the "F2 North complex" and

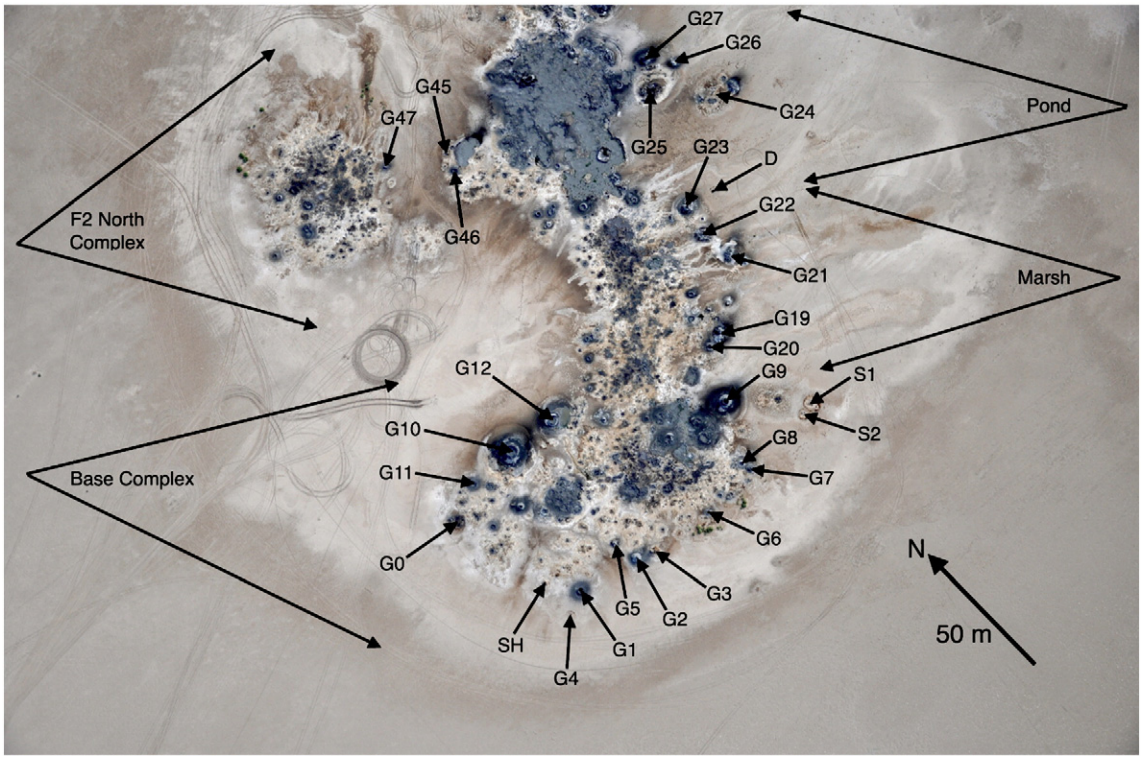

Fig. A2. F2, southwest section, annotated to identify gryphons, sales and regions with common geomorphology.

the “Base Complex”. Mud towers are found throughout F2, though hundreds of them cluster in the “marsh”, the “swamp” and on the north side of the “village”.

References

Anthony, J.W., Bideaux, R.A., Bladh, K.W., Nicols, M.C., 2003. Handbook of Mineralogy—Volume V. Borates, Carbonates, Sulfates, Mineral Data Publishing, Tucson (82 pp.).

Bonini, M., 2008. Elliptical mud volcano caldera as stress indicator in an active compressional setting (Nirano, Pede-Apennine margin, northern Italy). Geology 36, 131–134.

Bonini, M., 2009. Mud volcano eruptions and earthquakes in the Northern Apennines and Sicily, Italy. Tectonophysics 474, 723–735.

Brothers, D., Driscoll, N., Kent, G., Harding, A., Babcock, J., Baskin, R., 2009. Tectonic evolution of the Salton Sea inferred from seismic reflection data. Nature Geoscience 2, 581–584.

Dangermond, J., 2003. Salton Sea Atlas. ESRI Press, Redlands 136.

Delisle, G., von Rad, U., Andruleit, H., von Daniels, C.H., Tabrez, A.R., Inam, A., 2002. Active mud volcanoes on- and offshore eastern Makran, Pakistan. International Journal of Earth Sciences 91, 93–110.

Dewberry, Inc., 2011. “USGS Salton Sea LiDAR Project” USGS Contract: G10PC00013 Dewberry, 8401 Arlington Blvd. Fairfax, VA 22031-4666.

Dimitrov, L., 2002. Mud volcanoes—the most important pathway for degassing deeply buried sediments. Earth-Science Reviews 59, 49–76.

Elders, W.A., Cohen, L.H., 1983. The Salton Sea geothermal field, California, as a near-field natural analog of a radioactive waste repository in salt. Office of Nuclear Waste Isolation Rept. BMI/ONWI-513 (138 pp.).

Elders, W.A., Rex, R.W., Meidou, T., Robinson, P.T., Biehler, S., 1972. Crustal spreading in southern California. Science 178, 15–24.

Etiope, G., Feizullayev, A.A., Baciu, C.L., Milkov, A., 2004. Methane emission from mud volcanoes in eastern Azerbaijan. Geology 32, 465–468.

Fuis, Gary S., Mooney, W.D., 1990. Salton Trough lithospheric structure and tectonics from seismic-refraction and other data. In: Wallace, Robert E. (Ed.), The San Andreas Fault System, California: USGS Professional Paper, 1515 (Chapter 8).

Gurbuz, A., 2010. Geometric characteristics of pull-apart basins. Lithosphere 2, 199–206.

Hanks, H.G., 1882. Mud volcanoes and Colorado Desert. Second Report of the State Mineralogist of California; From December 1 1880 to Oct 1, 1882, Sacramento, pp. 227–240 (http://books.google.com/books?id=V1VJAAAAYAAJ&pg=PP7&lpg=PP7&dq=Second+Report+of+the+State+Mineralogist+of+California+1882&source=bl&ots=T3l5LNwaW-&sig=05QFGIZw-1KNO9UHT43y_1XC3TI&hl=en&sa=X&ei=BmBYUc7BIciZiQLznIGoAg&ved=0CC0Q6AEwAA).

Hauksson, E., Stock, J., Hutton, K., Yang, W., Vidal-Villegas, A., 2010. The 2010 Mw 7.2 El Mayor–Cucapah earthquake sequence, Baja California, Mexico and southernmost California, USA: active seismotectonics along the Mexican Pacific Margin. Pure and Applied Geophysics 168 (8–9), 1255–1277.

Helgeson, H., 1968. Geologic and thermodynamic characteristics of the Salton Sea geothermal system. American Journal of Science 266, 129–166.

Holdren, G.C., Montaño, A., 2002. Chemical and physical characteristics of the Salton Sea, California. Hydrobiologia 473 (1–3), 1–21.

Hovland, M., Hill, A., Stokes, D., 1997. The structure and geomorphology of the Dashgil mud volcano, Azerbaijan. Geomorphology 21, 1–15.

Hurlbert, Stuart H. (Ed.), 2008. The Salton Sea Centennial Symposium: Proceedings of a Symposium Celebrating a Century of Symbiosis Among Agriculture, Wildlife and People, 1905–2005, held in San Diego, California, USA, March 2005 Reprinted from HYDROBIOLOGIA, 604, p. 195 (VI).

Ives, R., 1951. Mud volcanoes of the Salton depression. Rocks and Minerals 26, 227–235.

Jakubov, A.A., AliZade, A.A., Zeinalov, M.M., 1971. Mud Volcanoes of the Azerbaijan SSR. Atlas. (in Russian) Azerbaijan Academy of Sciences, Baku.

Kennan, G., 1917. The Salton Sea: An Account of Harriman's Fight with the Colorado River. The MacMillan Company, New York 106.

Kopf, A., 2002. Significance of mud volcanism. Reviews of Geophysics 40 (2), 1–52.

Lachenbruch, A., Sass, J., Galanis, S., 1985. Heat flow in southernmost California and the origin of the Salton Trough. Journal of Geophysical Research 90, 6709–6736.

Larsen, E.S., Shannon, E.V., 1920. Boussingaultite from South Mountain, near Santa Paula, California. American Mineralogist 5, 127–128.

LeConte, J.L., 1855. Account of some volcanic springs in the desert of the Colorado, in Southern California. American Journal of Science No. 55 (XIX), 1–6 (2nd. Series, Jan 1855).

Lee, T.C., Cohen, L.H., 1979. Onshore and offshore measurements of temperature gradients in the Salton Sea geothermal area, California. Geophysics 44 (2), 206–215 (February).

Lonsdale, P., 1989. Geology and tectonic history of the Gulf of California. In: Winterer, E.L., Hussong, D.M., Decker, R.W. (Eds.), The Eastern Pacific Ocean and Hawaii: Geological Society of America, Decade of North American Geology, Boulder, Colorado, pp. 499–521 (v. N).

Lynch, D.K., 2011. The coming land bridge to Mullet Island. In: Reynolds, Robert E. (Ed.), Proceedings of the 2011 Desert Symposium, The Incredible Shrinking Pliocene, pp. 96–100 (April 22–25, 2011 Zzyzx).

Lynch, D.K., Hudnut, K.H., 2008. The Wister mud pot lineament: southeastward extension of abandoned strand of the San Andreas Fault? Bulletin of the Seismological Society of America 98, 1720–1729.

Lynch, D.K., Hudnut, K.H., Dearborn, D.S.P., 2010. Low altitude aerial color digital photographic survey of the San Andreas Fault in the Carrizo Plain. Seismological Research Letters 81, 453–459.

Macdonald, K.C., 1982. Mid-ocean ridges: fine scale tectonic, volcanic and hydrothermal processes within the plate boundary zone. Annual Review of Earth and Planetary Sciences 10, 155–190.

Magistrale, H., 2002. The relation of the southern San Jacinto fault zone to the Imperial and Cerro Prieto faults. Contributions to Crustal Evolution of the Southwestern United States. : GSA Special Paper, 365. Geological Society of America, Boulder, pp. 271–278.

Manga, M., Brumm, M., Rudolph, M., 2009. Earthquake triggering of mud volcanoes. Marine and Petroleum Geology 26, 1785–1798.

Mann, P., Hempton, M.R., Bradley, D.C., Burke, K., 1983. Development of pull-apart basins. Journal of Geology 91, 529–554.

Martinelli, G., Behrouz, P. (Eds.), 2003. Mud volcanoes, geodynamics and seismicity. Proceedings of the NATO Advanced Research Workshop on Mud Volcanism, Geodynamics and Seismicity, Baku, Azerbaijan, 20–22 May 2003: NATO Science Series: IV: Earth and Environmental Sciences, vol. 51.

Mazzini, A., Svensen, H., Planke, S., Guliyev, I., Akhmanov, G., Fallik, T., Banks, D., 2009a. When mud volcanoes sleep: insights from seep geochemistry at the Dashgil mud volcano, Azerbaijan. Marine and Petroleum Geology 26, 1704–1715.

Mazzini, A., Nermoen, A., Krotkiewski, M., Podladchikov, Y., Planke, S., Svensen, H., 2009b. Strike–slip faulting as a trigger mechanism for overpressure release through piercement structures. Implications for the Lusi mud volcano, Indonesia. Marine and Petroleum Geology 26, 1751–1765.

Mazzini, A., Svensen, H., Etiope, G., Onderdonk, N., Banks, D., 2011. Fluid origin, gas fluxes and plumbing system in the sediment-hosted Salton Sea Geothermal System (California, USA). Journal of Volcanology and Geothermal Research 205, 67–83.

Meltzner, A.J., Rockwell, T.K., Owen, L.A., 2006. Recent and long-term behavior of the Brawley Fault Zone, Imperial Valley, California: an escalation in slip rate? Bulletin of the Seismological Society of America 96 (6), 2304–2328.

Miller, S.R., Augustine, S., Olson, T.L., Blankenship, R.E., Selker, J., Wood, A.M., 2005. Discovery of a free-living chlorophyll d-producing cyanobacterium with a hybrid proteobacterial/cyanobacterial small subunit rRNA gene. Proceedings of the National Academy of Sciences of the United States of America 102 (3), 850–855. http://dx.doi.org/10.1073/pnas.0405667102.

Muffler, J., White, D., 1968. Origin of CO_2 in the Salton Sea geothermal system, southeastern California, U.S.A. Proc. Intl. Geol. Congress, 97 185–194.

Muffler, J., White, D., 1969. Active metamorphism of the upper Cenozoic sediments in the Salton Sea geothermal field and the Salton Trough, southern California. Geological Society of America Bulletin 80, 157–182.

Newark, R., Kasmeyer, P., Younker, L., 1988. Shallow drilling in the Salton Sea region: the thermal anomaly. Journal of Geophysical Research 93, 13005–13023.

Onderdonk, N., Shafer, L., Mazzini, A., Svensen, H., 2011. Controls on the geomorphic expression and evolution of gryphons, mud pots, and caldera features at hydrothermal seeps in the Salton Sea Geothermal Field, southern California. Geomorphology 130 (3–4), 327–342.

Pinch, W.W., 1978. Rare minerals report. Mineralogical Record 9 (2), 113–114.

Planke, S., Svensen, H., Hovland, M., Banks, D., Jamtveit, B., 2003. Mud and fluid migration in active mud volcanoes in Azerbaijan. Geo-Marine Letters 23, 258–268.

Quantification Settlement Agreement, 2003. http://bondaccountability.resources.ca.gov/plevel1.aspx?id=20&pid=4 www.fgc.ca.gov/.../Quantification%20Settlement%20Agreement.pdf.

Robinson, P.T., Elders, W.A., Muffler, L.J.P., 1976. Quaternary volcanism in the Salton Sea geothermal field, Imperial Valley, California. GSA Bulletin 87 (March), 347–360.

Rudolph, M., Manga, M., 2010. Mud volcano response to the 4 April 2010 El Mayor–Cucapah earthquake. Journal of Geophysical Research 115, B12211.

Schmitt, A.K., Vazquez, J., 2006. Alteration and remelting of nascent oceanic crust during continental rupture: evidence from zircon geochemistry of rhyolites and xenoliths from the Salton Trough, California. Earth and Planetary Science Letters 252 (3–4), 260–274.

Sturz, A., Kamps, R., Earley, P., 1992. Temporal changes in mud volcanoes, Salta Sea geothermal area. In: Kharaka, Y., Maest, A. (Eds.), Water–Rock Interaction. Balkema, Rotterdam, Netherlands, pp. 1363–1366.

Sturz, A., Itoh, M., Earley, P., Otero, M., 1997. Mud volcanoes and mud pots, Salton Sea geothermal area, Imperial Valley, California. In: Deen, P., Metzler, C., Trujillo, A. (Eds.), Geology and Paleontology of the Anza-Borrego Region, California. Field Trip Guidebook for the National Association of Geoscience Teachers Far Western Section, 1997 Spring Field Conference (pages).

Svensen, H., Karlsen, D., Sturz, A., Backer-Owe, K., Banks, D., Planke, S., 2007. Processes controlling water and hydrocarbon composition in seeps from the Salton Sea geothermal system, California, USA. Geology 35, 85–88.

Svensen, H., Hammer, Ø., Mazzini, A., Onderdonk, N., Polteau, S., Planke, S., Podladchikov, Y.Y., 2009. Dynamics of hydrothermal seeps from the Salton Sea geothermal system (California, USA) constrained by temperature monitoring and time series analysis. Journal of Geophysical Research 114 (B9), B09201.

Taylor, W.J., 1858. Mineralogical notes. Proceedings of the Academy of Natural Sciences of Philadelphia 10, 172 (http://books.google.com/books?id=xuxBm9kg1YwC&printsec=frontcover&source=gbs_ge_summary_r&cad=0#v=onepage&q&f=false).

Tratt, D.M., Lynch, D.K., 2010. Earth Science Picture of the Day (EPOD). http://epod.usra.edu/blog/2010/08/salton-sea-geothermal-features-1.html.

Tratt, D.M., Young, S.J., Lynch, D.K., Buckland, K.N., Johnson, P.D., Hall, J.L., Westberg, K.R., Polak, M.L., Kasper, B.P., Qian, J., 2011. Remotely-sensed ammonia emission from fumarolic vents associated with a hydrothermally active fault in the Salton Sea Geothermal Field, California. Journal of Geophysical Research—Atmospheres 116, D21308.

Veatch, J., 1860. Salses or mud volcanoes of the Colorado Desert. Hesperian 3, 481–489.
Wang, H., Dalla, I.G., Chuang, L., Chuang, K.T., 2008. Thermodynamics and stoichiometry of reactions between hydrogen sulfide and concentrated sulfuric acid. The Canadian Journal of Chemical Engineering 81 (1), 80–85.
Westmoreland Gauge, 2011. http://waterdata.usgs.gov/nwis/dv?referred_module=sw&site_no=10254005.
Winchell, H., Benoit, R.J., 1951. Taylorite, mascagnite, aphthitalite, lecontite, and oxammite from guano. American Mineralogist 36, 591.
Younker, L.W., Kasameyer, P.W., Tewhey, J.D., 1982. Geological, geophysical and thermal characteristics of the Salton Sea geothermal field, California. Journal of Volcanology and Geothermal Research 12 (3–4), 221–258.